Magnetic Resonance Imaging 62 (2019) 1–9

Contents lists available at ScienceDirect

Magnetic Resonance Imaging

journal homepage: www.elsevier.com/locate/mri

Original contribution

Dynamics of blood brain barrier permeability and tissue microstructure following controlled cortical impact injury in rat: A dynamic contrast-enhanced magnetic resonance imaging and diffusion kurtosis imaging study

Mengmeng Yu[a,1], Mingliang Wang[a,1], Dianxu Yang[b], Xiaoer Wei[a], Wenbin Li[a,c,*]

[a] Department of Radiology, Shanghai Jiao Tong University Affiliated Sixth People's Hospital, 600 Yishan Road, Shanghai 200233, China
[b] Department of Neurosurgery, Shanghai Jiao Tong University Affiliated Sixth People's Hospital, 600 Yishan Road, Shanghai 200233, China
[c] Imaging Center, Kashgar Prefecture Second People's Hospital, Kashgar 844000, Xinjiang, China

ARTICLE INFO

Keywords:
Traumatic brain injury
Blood-brain barrier
Diffusion kurtosis imaging
Dynamic contrast-enhanced MRI
Thalamus

ABSTRACT

Objective: The blood-brain barrier (BBB) and cerebral tissue microstructure can be impaired following traumatic brain injury (TBI). However, the spatiotemporal changes of BBB leakage and tissue microstructure are not completely understood. In this study, we evaluated the spatiotemporal changes of BBB leakage and tissue microstructure using dynamic contrast-enhanced magnetic resonance imaging (DCE-MRI) and diffusion kurtosis imaging (DKI) in controlled cortical impact (CCI) rats.

Materials and methods: The DCE-MRI parameters volume transfer coefficient (K^{trans}) and DKI parameters were longitudinally measured in bilateral cortex, hippocampus, thalamus and corpus callosum (CC) at baseline (D0), acute stage (D1, D3), and subacute stage (D7, D14 and D28) post-injury. Immunohistochemistry analysis was performed at D28 after MRI scanning. Repeated-measures ANOVA was used to assess the temporal changes of MRI parameters.

Results: K^{trans} abnormality was only localized to ipsilateral perilesional cortex with a significant temporal change ($F = 144.2$, $p < 0.0001$). Compared to baseline, increased mean kurtosis (MK) was observed in ipsilateral regions of cortex and hippocampus and CC for all the time points ($p < 0.05$ for all). Increased MK was also observed in ipsilateral thalamus ($p = 0.005$) at subacute stage but not at acute stage while no change was observed with MD and FA ($p > 0.05$ for both). In ipsilateral cortex, the overall K^{trans} value of D0, D1, D3, D7, D14, and D28 post-injury were significantly correlated with MK value ($r = 0.84$, $p < 0.0001$). The CCI group showed higher staining of glial fibrillary acidic protein (GFAP) and ionized calcium binding adaptor molecule 1 (Iba-1) and lower staining of neuron-specific nuclear protein (NeuN) and myelin basic protein (MBP) in ipsilateral regions of cortex, hippocampus, thalamus and CC ($p < 0.05$ for all) as compared to control group. There were no significant differences in the contralateral regions by immunohistochemistry.

Conclusion: The BBB disruption reflected by K^{trans} correlated well with MK value in ipsilateral cortex. In addition, MK could detect the delayed microstructural changes in thalamus. DCE-MRI and DKI could be used to assess the BBB breakdown and cerebral microstructural changes of TBI.

1. Introduction

Traumatic brain injury (TBI) is one of the leading causes of death and disability worldwide, with a high incidence in military and civilian populations [1]. The pathology of TBI is highly heterogeneous, with diverse manifestations that result from primary and secondary injuries [2]. Experimental studies have demonstrated that blood-brain barrier (BBB) breakdown is involved in the initiation of transcriptional changes in the neurovascular network that ultimately lead to delayed neuronal dysfunction and degeneration [3,4]. Moreover, acute dysfunction of the neurovascular unit may be a common pathological feature, even for concussion [5]. Once injury events are initiated, interaction between them may influence the ongoing brain damage, which suggests a dynamic pathophysiological evolvement in time and space.

Magnetic resonance imaging (MRI) is increasingly used to assess the progression of TBI. Diffusion tensor imaging (DTI) is a powerful tool for

* Corresponding author at: Department of Radiology, Shanghai Jiao Tong University Affiliated Sixth People's Hospital, 600 Yishan Road, Shanghai 200233, China.
E-mail address: liwenbin@stju.edu.cn (W. Li).
[1] Dr. Mengmeng Yu and Dr. Mingliang Wang contributed equally to the manuscript.

https://doi.org/10.1016/j.mri.2019.01.017
Received 6 December 2018; Received in revised form 15 January 2019; Accepted 16 January 2019

detecting cerebral microstructural changes after injury. DTI assumes a Gaussian distribution for the water molecule in measured tissue [6]. However, the true movement of water molecules is non-Gaussian in distribution. Therefore, DTI technique might not capture the real microstructural pathologic changes, especially for the largely isotropic gray matter. Diffusion kurtosis imaging (DKI) could overcome this limitation, since it extends DTI by quantifying non-Gaussian model of water diffusion [7]. Currently, DKI has been widely applied in detecting brain microstructural alterations in TBI. Previous studies have found mean kurtosis (MK), which measures the average kurtosis, to be a marker for tissue complexity or heterogeneity [8]. An increase of MK may be associated with reactive astrogliosis in acute and subacute TBI [9]. Decreased MK may be observed in chronic TBI indicative of neuron loss, microgliosis, and myelin disruption [10]. Dynamic contrast-enhanced magnetic resonance imaging (DCE-MRI) is a noninvasive perfusion MRI technique. The DCE-MRI parameter volume transfer coefficient (K^{trans}) value can quantitatively measure BBB permeability, and was considered as an in vivo biomarker of BBB disruption [11]. Prior animal studies have utilized DCE-MRI to longitudinally assess BBB opening in TBI [12,13]. A recent human research demonstrated BBB breakdown could be responsible in the development of PCS in mild TBI patients, which can be detected by K^{trans} value [14].

To date, however, most studies have primarily focused on either BBB leakage [4,14] or cerebral tissue alteration [9,10,15]. The relationship between the BBB permeability and brain microstructural changes post-injury has been rarely studied [16]. Therefore, the aim of this study was to use DCE-MRI and DKI to investigate whether BBB permeability correlated with cerebral tissue microstructural changes. Knowledge of these interactions may facilitate a better understanding of their roles in mediating cerebral injury and restorative processes.

2. Experimental procedures

This study was approved by the institutional animal research committee, and conducted in accordance with the guidelines of the International Council on Animal Care. All animals were housed in plastic cages under a 12-hour light/dark cycle, with free access to water and food. Eight adult male Sprague-Dawley rats (250–300 g/8 weeks) were subjected to right parietal controlled cortical impact (CCI) injury and underwent longitudinal MRI examinations at baseline, day 1, 3, 7, 14 and 28 post-injury. Three additional control rats (250–300 g/8 weeks) without impact intervention were included. After all imaging examinations were completed, the CCI rats and three control rats were used for immunohistochemistry (IHC) analysis.

2.1. CCI rat model

The TBI was induced by CCI impact device (PinPoint Precision Cortical Impactor PCI3000, Hatteras Instruments Inc.; Cary, NC). Briefly, rats were anesthetized with ketamine and then placed in a stereotaxic holder. A midline incision (10 mm in length) was made over the skull, and craniotomy was performed using a 4 mm trephine centered at 3.5 mm posterior and 4 mm right lateral to bregma, exposing the dura matter. When performing the operation, care was taken to maintain an intact dura; if dural integrity was breached, the rat was excluded from the study [17,18]. After the intact dura was exposed, the injury was created using a 3-mm-diameter rounded steel impactor tip of a CCI device. The CCI parameters were as follows: tip diameter = 3 mm, velocity = 1.5 m/s, deformation depth = 1.5 mm, and dwell time = 100 ms. Following the injury, the cranial opening was sealed with bone wax. Three control rats underwent the same craniotomy operation without impact intervention.

2.2. MRI

MRI was performed on a Bruker Biospec 7.0 Tesla 20 cm horizontal bore scanner (Bruker Biospin MRI GmbH, Germany). The eight CCI rats and three control rats underwent MRI scanning. During the scan, the animal was under 1–2% isoflurane anaesthesia and 1 L/min oxygen administration. The animal was secured in a custom-built MRI-compatible rat head stereotaxic holder with ear and tooth bars. All rats underwent T2-weighted, DKI and DCE-MRI examinations at baseline and day 1, 3, 7, 14 and 28 after injury. The total duration of the entire imaging experiment was approximately 1 h for each rat.

A multi-echo 2D Rapid Acquisition with Relaxation Enhancement (RARE) sequence was used to acquire T2-weighted images with the following parameters: TR = 4500 ms, TE = 20, 60, 100, 140 ms, rare factor = 2, FOV = 30 × 30 mm; matrix = 128 × 128, with slice thickness = 1 mm. The DKI sequence was carried out by a spin-echo echo-planar imaging (EPI) diffusion sequence with two repetitions, using 20 different diffusion encoding directions. For each direction, four b-values (b = 0, 650, 1300, 2000 s/mm^2) were acquired. Other imaging parameters were as follows: TR/TE = 3500/50 ms; δ/Δ = 5/18 ms; 19 axial slices; slice thickness = 1 mm; FOV = 30 × 30 mm; matrix = 128 × 128. Then, 3D T1 high-resolution isotropic volume excitation (3D-THRIVE) was used to complete the DCE-MRI. The parameters for the 3D-THRIVE sequence used in DCE-MRI were: TR/TE = 32/1.8 ms, spatial resolution = 0.23 × 0.23 × 0.23 mm. Before the DCE-MRI scans, the 3D-THRIVE sequence with FA (flip angle) = 8° was scanned for one phase. Then the 3D-THRIVE sequence was dynamically scanned for 120 phases for DCE-MRI. The 8° and 12° FA and the same TR/TE were used to generate the T1 maps. During the DCE-MRI scanning, after the pre-contrast baseline scans, animals were intravenously injected with Gd-DTPA (0.1 mmol/kg) through the tail vein. The total scan time for 120 3D-THRIVE sequences was 8.2 min.

2.3. Imaging analysis

DKI data were processed by the Diffusion Kurtosis Estimator software (DKE) (https://www.nitrc.org/projects/dke/). The DKI parametric maps included MK, MD and FA, which could be generated by this software [19]. The ROIs, including ipsilateral and contralateral areas to the injury in the cortex, bilateral hippocampus, bilateral thalamus and corpus callosum (CC), were defined on T2-weighted images on three consecutive slices using ITK-SNAP software [20] (www.itksnap.org) (Fig. 1A–B). Then ROIs were manually drawn on the b = 0 images and transferred to identical sites on other FA, MD and MK maps (Fig. 1C–D). The perilesional area in cortex refers to the ipsilateral parietal area excluding the core lesion area. We avoided the hemorrhage areas and excluded its influence, when drawing the ROIs [9]. ROIs were sufficiently large but not defined to the edge of the tissues on the section. A single voxel width was used for the delineation of corpus callosum. The average regional value for each DKI parameter was recorded from the voxels within each ROI.

All DCE-MRI were transmitted to image-analysis software (CINEtool; GE Healthcare, Milwaukee, Wisconsin) to obtain quantitative K^{trans} values for DCE-MRI, with the middle cerebral artery as the input artery. According to previous methods [12,13], the K^{trans} value was calculated by the two-chamber model [21]. ROIs were defined on the basis of T2-weighted images on three consecutive slices, and manually drawn on the K^{trans} map with cautious. The K^{trans} values of the different regions were calculated. The procedures were performed by two radiologists, who were blinded to the time and independently drew the ROIs.

2.4. IHC staining and quantitative analysis

After the final MRI scanning, the CCI and control rats were deeply anesthetized with ketamine and transcardially perfused with saline followed by 4% paraformaldehyde. Then the brains were extracted, post-fixed, dehydrated with alcohols, and embedded in paraffin. Subsequently, three serial axial sections (4 μm) were made surrounding

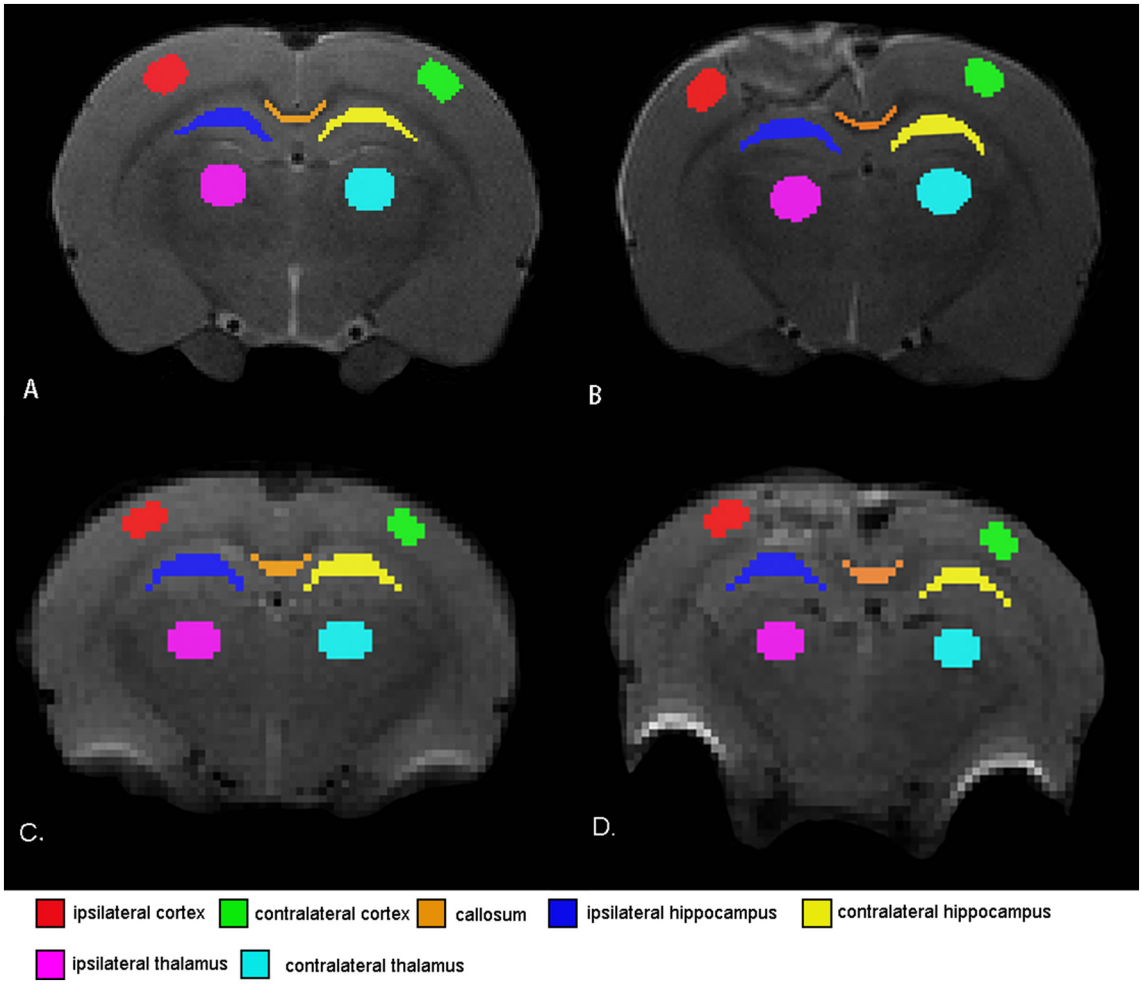

Fig. 1. Illustration of ROIs on T2-weighted images (A, B) and b = 0 images (C, D) for a representative rat at baseline and 28 days post-injury, respectively. Regions shown are bilateral cortex (ips, con), bilateral hippocampus (ips, con), bilateral thalamus (ips, con) and callosum (ips, con) (ips = ipsilateral; con = contralateral).

the lesion site in the brain, which was similar to the section of MRI analysis. IHC staining was performed on these coronal sections, using established neuronal markers (NeuN; 1:100; Servicebio, Wuhan), astroglia (GFAP; 1:400; Servicebio, Wuhan), microglia (Iba-1; 1:1000; Servicebio, Wuhan), and myelin (MBP; 1:100; Servicebio, Wuhan).

Sections were analyzed under the microscope (Dewinter, Germany) and IHC images were captured for cell counting. Brain images were obtained and quantified for the number of $NeuN^+$, $GFAP^+$, Iba-1^+ cells and the IHC staining area of MBP^+. In order to maximally match the MRI measured area, three random FOV of three serial sections at a magnification of 40× were taken to quantify the IHC results. The mean of these values was used to calculate the mean positive cell numbers or area percentage in each region. The positively stained cells or staining area was manually counted using a computer-based image analysis system (ImageJ 1.51, Wayne Rasband, National Institutes of Health, Bethesda, USA). The same protocol was used for the two groups.

2.5. Statistical analysis

Statistical analysis was performed by the Statistical Package for Social Sciences (IBM Corp, Armonk, NY, USA) software for Windows version 20.0, and graphs were plotted using GraphPad Prism 6.0 software (GraphPad Software, Inc., USA). The DKI and K^{trans} parameters are presented as mean ± standard deviation (SD), and the IHC data are expressed as the mean ± standard error of the mean (SEM). The DKI parameters and K^{trans} values were compared by repeated-measures ANOVA, followed by paired *t*-tests. Differences in IHC data were analyzed using Student's *t*-tests. The correlations between DKI parameters and K^{trans} were calculated by Spearman's test. Statistical significance was defined as $p < 0.05$.

3. Results

3.1. DCE and DKI parameter changes in CCI rats

Fig. 2 shows T2W, fractional anisotropy (FA), mean diffusivity (MD), MK and DCE-MRI images from a representative rat at all time points from baseline to 28 days after CCI injury. Figs. 3–4 show the changes in longitudinal K^{trans} and DKI parameters.

3.1.1. Regional and temporal changes of K^{trans}

In the CCI group, the K^{trans} changes were only localized to ipsilateral cortical layers around the site of injury, while no abnormal K^{trans} changes were observed in ipsilateral regions of hippocampus and thalamus. In corpus callosum and contralateral hemisphere, K^{trans} was not affected across all time-points. The K^{trans} of perilesional areas in cortical layer showed a significant temporal change ($F = 144.2$, $p < 0.0001$). Specifically, K^{trans} increased at day 1 ($p < 0.001$), peaked at day 3 ($p < 0.001$), and subsequently decreased at day 7 ($p < 0.001$), 14 ($p < 0.001$) and 28 ($p < 0.001$) post-injury but remained significantly elevated (Fig. 3A).

In the control group, no significant differences were observed in callosum, bilateral hippocampus, thalamus and cortex as compared to baseline (online Fig. 1A–D), indicating that the changes of K^{trans} in CCI

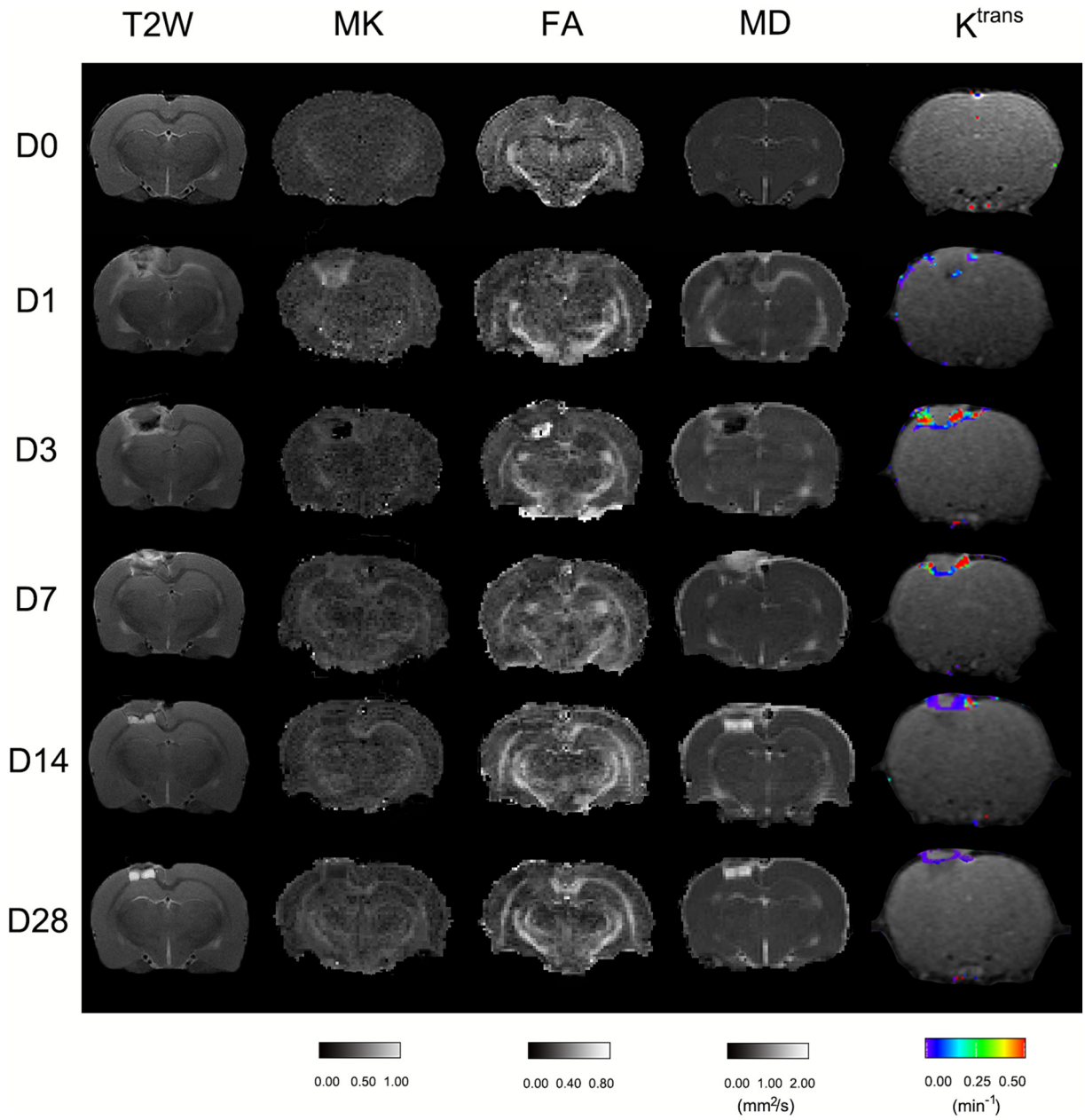

Fig. 2. T2W, FA, MD, MK and K^{trans} maps from the same rat brain at baseline and day 1, 3, 7, 14 and 28 after TBI.

group was not affected by craniotomy and anaesthesia.

3.1.2. Regional and temporal changes of DKI parameters

3.1.2.1. CCI group. Callosum, bilateral hippocampus, ipsilateral thalamus and cortex experienced significant increase in MK during the 28 days trial (hip_ips: $F = 36.90$, $p < 0.001$; hip_con: $F = 7.09$, $p < 0.001$; tha_ips $F = 3.75$, $p = 0.011$; cortex_ips: $F = 25.38$, $p < 0.001$; callosum: $F = 13.74$, $p = 0.001$). The contralateral regions of cortex and thalamus (cortex_con: $F = 0.88$, $p = 0.51$; tha_con: $F = 0.74$, $p = 0.68$) showed no significant changes in MK values, indicating a spatial gradient in MK impairment moving away from the site of injury. Notably, at day 14 post-injury, there was a significant increase of MK in the ipsilateral thalamus ($p = 0.005$) and contralateral hippocampus ($p = 0.005$) as compared to baseline, indicating the spread of neurodegenerative processes to the deep gray matter after injury (Fig. 4B–C). In ipsilateral cortex, the temporal changes of MK showed the same trend as ipsilateral K^{trans}, elevating at day 1 ($p < 0.001$), peaking at day 3 ($p < 0.001$) and then declining at subacute stage ($p < 0.05$).

For FA, the time effect was significant for hip_ips ($F = 8.72$, $p = 0.030$) and callosum ($F = 11.30$, $p < 0.001$). CCI injury induced a significant reduction in FA in callosum at day 1, 3, 7, 14 ($p < 0.05$ for all). The ipsilateral hippocampus ($p = 0.009$) showed a significant increase at day 7 post-injury, and then gradually recovered to baseline (Fig. 4F).

For MD, significant changes with time were observed in the ipsilateral regions of cortex ($F = 47.20$, $p < 0.001$), hippocampus ($F = 10.32$, $p < 0.001$), and callosum ($F = 10.73$, $p < 0.001$). MD was significantly increased in callosum at all time points. In the ipsilateral cortex, MD slightly declined at day 1 ($p = 0.08$), then significantly peaked on day 3 ($p < 0.001$) and subsequently decreased at day 7 ($p = 0.021$) and declined towards baseline at day 28 ($p = 0.11$) (Fig. 4I). The ipsilateral hippocampus showed markedly higher MD at day 3 ($p < 0.001$) post-injury.

3.1.2.2. Control group

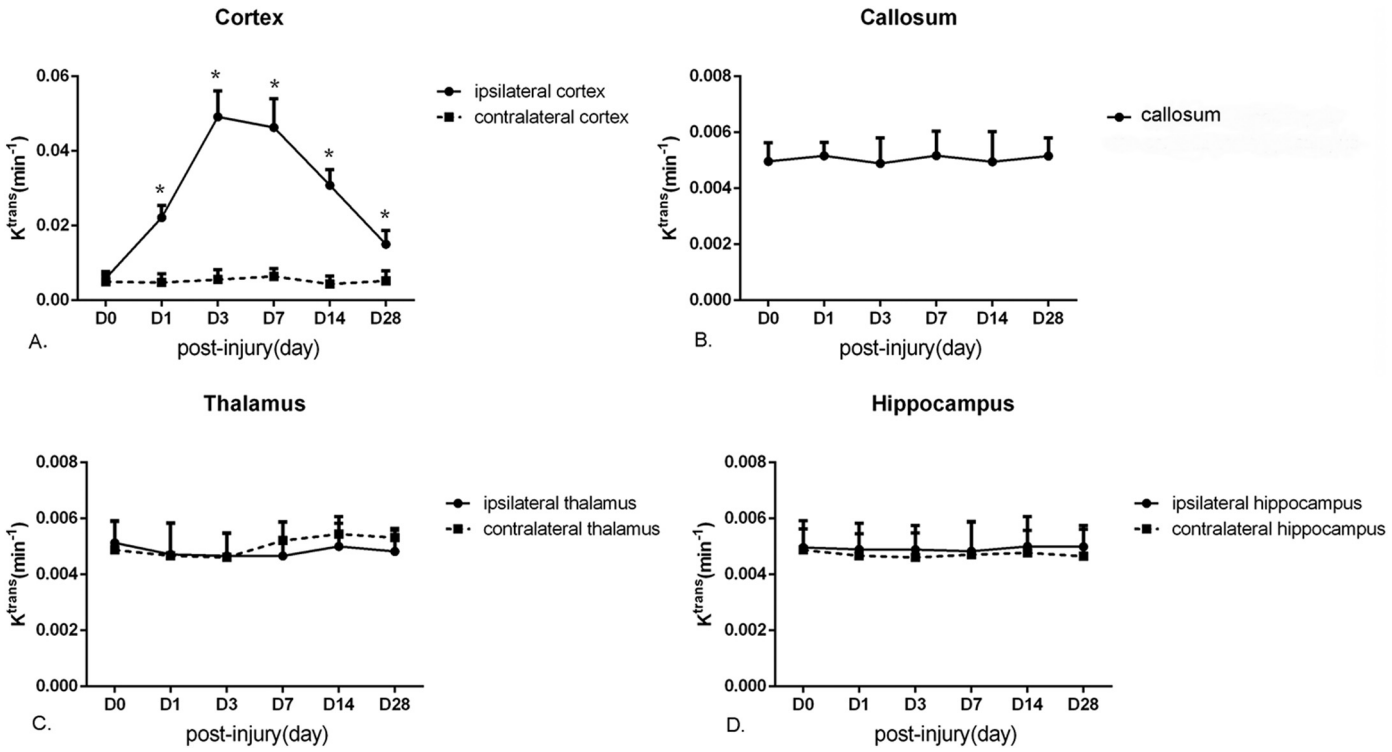

Fig. 3. K^{trans} in bilateral cortex (ips, con), bilateral hippocampus (ips, con), bilateral thalamus (ips, con) and callosum at baseline and day 1, 3, 7 and 28 post-injury in the CCI group. Error bars indicate standard deviation. Asterisk indicates $p < 0.05$ as compared to baseline by repeated-measures ANOVA followed by paired *t*-tests (ips = ipsilateral; con = contralateral).

In control group, no significant differences were observed in MK, FA and MD values as compared to baseline in all the ROIs (online Fig. 2A–C), indicating that the changes of FA, MD and MK in CCI group was not affected by craniotomy and anaesthesia.

3.1.3. Correlation between K^{trans} and DKI parameters

In ipsilateral cortex, Spearman's correlation analysis demonstrated that MK correlated well with K^{trans} ($r = 0.84$, $p < 0.0001$), whereas other parameters showed poor correlation (FA: $r = -0.177$, $p = 0.228$; MD: $r = 0.46$, $p = 0.002$) (Fig. 5A–C).

3.2. IHC quantitative analysis at day 28 post-injury

Online Fig. 3(A–C) shows the representative IHC staining images of $NeuN^+$, $GFAP^+$, Iba-1^+, and MBP^+ in the bilateral cortex, hippocampus, thalamus and callosum in a control and CCI rat brain section. Fig. 6(A–D) shows the IHC staining changes at day 28 post-injury.

The ipsilateral regions of cortex, hippocampus and thalamus revealed lower IHC staining of $NeuN^+$ and MBP^+, and higher IHC staining of $GFAP^+$ and Iba-1^+ in the CCI group ($p < 0.001$ for all). In callosum, GFAP ($p < 0.001$) and Iba-1 ($p < 0.001$) cells significantly increased and MBP ($p = 0.004$) decreased. However, there were no significant differences in contralateral regions of cortex, hippocampus and thalamus ($p > 0.05$ for all).

4. Discussion

In this study, we used DCE-MRI and DKI to evaluate the dynamic changes of BBB permeability and cerebral microstructure in a CCI rat model. The results showed that: (1) abnormal K^{trans} was only observed in ipsilateral cortical layers around the lesion site; (2) in the ipsilateral perilesional cortex, MK value correlated well with K^{trans} value, while FA and MD showed poor correlation; and (3) The CCI rat model triggers delayed MK abnormality in ipsilateral thalamus.

4.1. BBB breakdown localized in ipsilateral cortical layer around the lesion site

Animal studies and clinical trials have demonstrated that head trauma frequently causes BBB breakdown [13,22]. Our results supported this finding, since K^{trans} values were significantly increased at all the time points post-injury as compared to baseline. Our results are also in line with previous studies, which reported that K^{trans} increased at day 1, peaked at day 3 and began to decline at day 7 post-injury [13,16].

However, this study found that BBB breakdown induced by CCI injury was localized only in ipsilateral cortex surrounding the impacted site, not the widespread changes observed by DKI parameters in both cortical layer and deep regions. Recently, Johnson et al. demonstrated the extensive disruption of BBB in bilateral hemisphere in a swine concussion model [5]. This discrepancy may be due to that head rotational acceleration force of concussion, which can induce a wider injury area as compared to that of our CCI device.

4.2. MK value correlated well with K^{trans} in the ipsilateral perilesional cortex

A strong positive correlation was observed between K^{trans} and MK value in ipsilateral cortex, while FA and MD showed poor correlation. Consistent with a previous DTI study [16], Li et al. found that K^{trans} value did not correlate with FA changes. Our current study extended Li et al.'s. study by utilizing DKI to investigate the relationship between K^{trans} and diffusion parameters.

The impairment of BBB increased permeability from the blood vessels to the extracellular space, led to tissue accumulation of potentially neurotoxic blood-derived products and triggered a series of pathological changes, including glial proliferation, neuronal loss and myelin disruption [14,22]. Similar to previous findings, the ipsilateral perilesional cortex had increased $GFAP^+$ and Iba-1^+ cells [23,24]. These changes would increase microstructural complexity, thereby

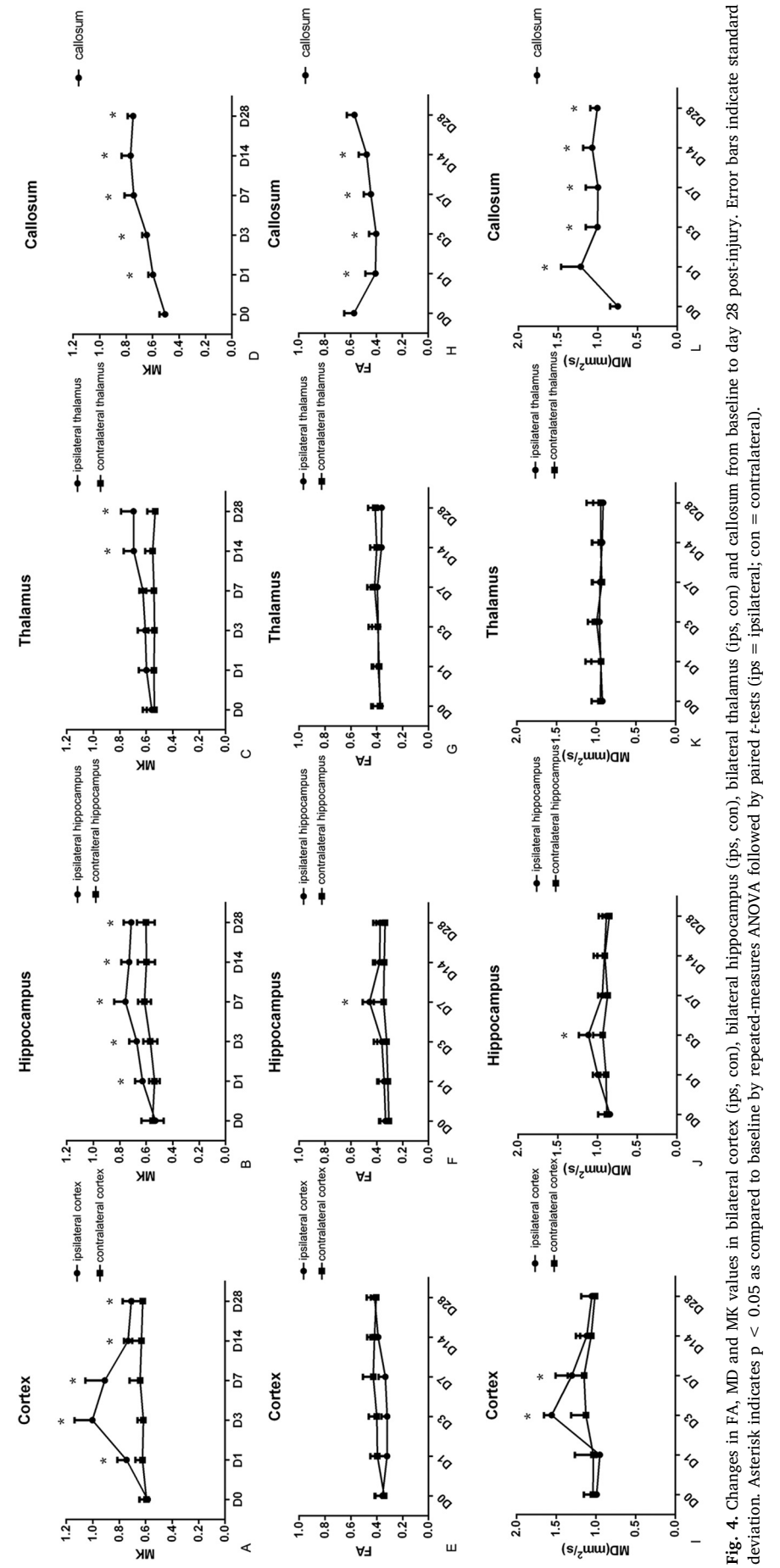

Fig. 4. Changes in FA, MD and MK values in bilateral cortex (ips, con), bilateral hippocampus (ips, con), bilateral thalamus (ips, con) and callosum from baseline to day 28 post-injury. Error bars indicate standard deviation. Asterisk indicates $p < 0.05$ as compared to baseline by repeated-measures ANOVA followed by paired *t*-tests (ips = ipsilateral; con = contralateral).

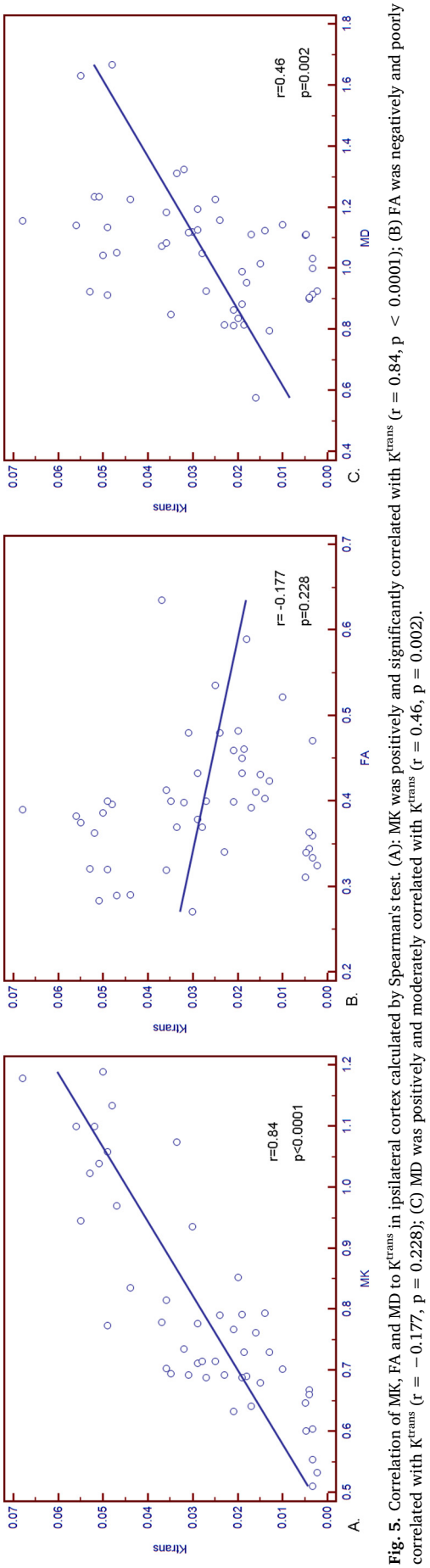

Fig. 5. Correlation of MK, FA and MD to K^{trans} in ipsilateral cortex calculated by Spearman's test. (A): MK was positively and significantly correlated with K^{trans} ($r = 0.84$, $p < 0.0001$); (B) FA was negatively and poorly correlated with K^{trans} ($r = -0.177$, $p = 0.228$); (C) MD was positively and moderately correlated with K^{trans} ($r = 0.46$, $p = 0.002$).

elevating MK value. Our study also revealed decreased $NeuN^+$, and MBP^+ staining in the ipsilateral perilesional cortex, which was consistent with previous studies [23,24]. Notably, neuronal loss and myelin disruption will loosen cellular structure, which seemed to lower MK value. Previous studies suggested that the voxel diffusion signal is a summation of all brain microstructural effects [15,25]. We speculated that the effect of neuronal loss and myelin disruption on lowering MK value might be smaller than microgliosis and astrogliosis on elevating the MK value at an early stage. However, the combined effect of glial proliferation, neuronal loss and myelin disruption may essentially offset any changes in DTI parameters. Thus, poor relationship was observed between DTI and K^{trans}. Taken together, these microstructural pathological changes resulting from BBB disruption caused increased microstructural complexity and correlated with MK changes. Overall, BBB breakdown may be linked to neuronal dysfunction and degeneration.

4.3. CCI rat model triggers delayed MK elevation in ipsilateral thalamus

Notably, this study found a significant MK increase in ipsilateral thalamus at subacute stage but not at acute stage. However, MD and FA remained relatively unchanged in thalamus across all time-points, indicating that MK is more sensitive for detecting microstructural changes in gray matter.

As for the underlying pathological changes, the study showed increased $GFAP^+$ and $Iba\text{-}1^+$, and decreased $NeuN^+$ and MBP^+ in ipsilateral thalamus at day 28. The effect of neuronal loss and myelin disruption in lowering MK value might be smaller than microgliosis and astrogliosis in elevating the MK value at early stage. Therefore, MK value might mainly result from the proliferation of astrocytes and microglia, and DKI could provide additional information about subcortical nuclei post-injury. This finding was consistent with a previous study, which found that astrocytosis occurred rapidly at the site of cortical injury, but was delayed in thalamus [26,27].

The exact underlying neurobiological mechanisms still controversial. Prior studies attributed thalamus injury to retrograde axonal degeneration of thalamo-cortical connections [28–31]. Grossman et al. speculated both primary injury from TBI and secondary injury from white matter injury could lead to thalamic damage [32]. However, a recent football player of repetitive head impacts research [33] found that no significant difference of FA was observed in white matter fibers, indicating the connecting tracts was integrity. Therefore, further studies are still needed to unmask the underlying mechanisms.

The injury of thalamus in TBI may lead to some long-term symptoms, such as cognitive impairment [32,34] and sleep disruptions [26]. Thus, it is important to monitor thalamus damage after TBI. Taken together, this study suggested that DKI can be used as a noninvasive method to detect delayed neurodegeneration in thalamus and determine possible targets for treatment.

A prior human study found significant reduction of MK in the thalamus of patients with mild TBI as compared to healthy participants [32]. Also, decreased MK was observed in football players with repetitive impacts [33]. These findings are not contradictory to the results of our study since MK changes as the disease progresses. Most patients included in previous studies had subacute or chronic TBI. With the progression of disease, the proliferation of astrocytes may be less and the extracellular space may be increased at a more chronic stage [35,36]. These pathological changes can cause significant reduction in the degree of tissue complexity, thereby reducing MK. Microenvironmental changes may occur as a result of numerous cellular processes during the course of tissue recovery and MK, therefore, is likely to depend on the time elapsed post-injury.

This study had several limitations. First, this was a longitudinal study and all the rats underwent MRI scanning at five different time points. Considering the five scans at different time points, each slice and ROIs were inevitably not identical. However, this study used T2-weighted image as the anatomical reference to define ROIs, in order to

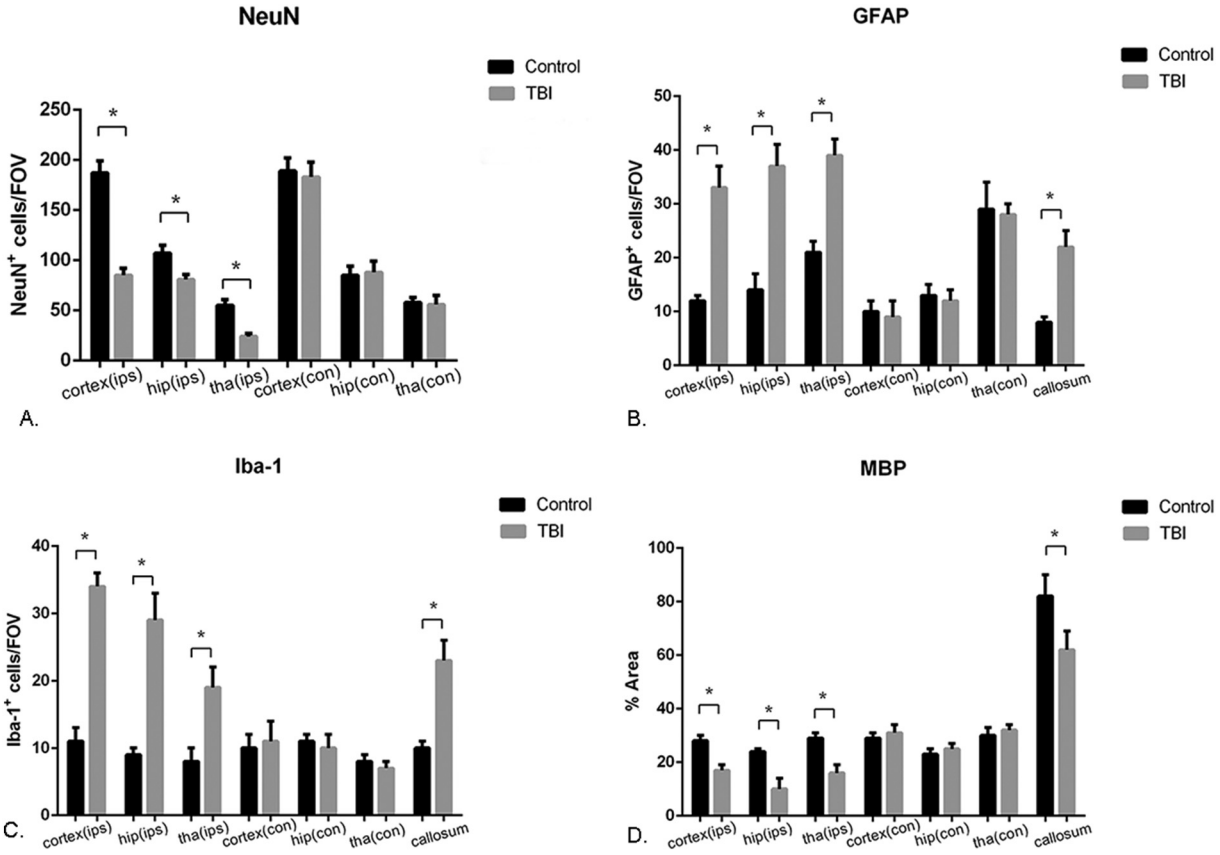

Fig. 6. Changes in NeuN$^+$, GFAP$^+$, and Iba-1$^+$ cells and MBP$^+$ area in the bilateral cortex (ips, con), bilateral hippocampus (ips, con), bilateral thalamus (ips, con) and corpus callosum. Error bars indicate standard error of mean (SEM). Asterisk indicates $p < 0.05$ as compared to the control group by Student's *t*-test (ips = ipsilateral; con = contralateral).

ensure that the ROIs remained relatively at the same location in each rat during the 28-day trial. Second, we did not quantitatively evaluate neurofunction, since TBI was often accompanied by some neurofunctional impairment. Third, the follow-up time was relatively short, only 28 days post-injury. Thus, further radiological-pathological studies are needed to confirm the findings.

5. Conclusion

The BBB disruption reflected by K^{trans} correlated well with MK value in ipsilateral cortex. In addition, MK could detect the delayed neurodegeneration in thalamus. Therefore, DCE-MRI and DKI could be useful tools in the evaluation of BBB breakdown and cerebral microstructural changes of TBI.

Supplementary data to this article can be found online at https://doi.org/10.1016/j.mri.2019.01.017.

Competing interests

The authors declare that they have no competing interests.

Funding sources

This study was funded by the National Natural Science Foundation of China (grant number: 81271540), Natural Science Foundation of Xinjiang Province (grant number: 2016D01C083) and Shanghai Key Discipline of Medical Imaging (grant number: 2017ZZ02005).

References

[1] Bruns Jr. J, Hauser WA. The epidemiology of traumatic brain injury: a review. Epilepsia 2003;44(s10):2–10.
[2] Le TH, Gean AD. Neuroimaging of traumatic brain injury. Mt Sinai J Med 2009;76(2):145–62.
[3] Shlosberg D, Benifla M, Kaufer D, Friedman A. Blood-brain barrier breakdown as a therapeutic target in traumatic brain injury. Nat Rev Neurol 2010;6(7):393–403.
[4] Pop V, Sorensen DW, Kamper JE, Ajao DO, Murphy MP, Head E, et al. Early brain injury alters the blood-brain barrier phenotype in parallel with beta-amyloid and cognitive changes in adulthood. J Cereb Blood Flow Metab 2013;33(2):205–14.
[5] Johnson VE, Weber MT, Xiao R, Cullen DK, Meaney DF, Stewart W, et al. Mechanical disruption of the blood-brain barrier following experimental concussion. Acta Neuropathol 2018;135(5):711–26.
[6] Basser PJ, Mattiello J, LeBihan D. MR diffusion tensor spectroscopy and imaging. Biophys J 1994;66(1):259–67.
[7] Jensen JH, Helpern JA, Ramani A, Lu H, Kaczynski K. Diffusional kurtosis imaging: the quantification of non-Gaussian water diffusion by means of magnetic resonance imaging. Magn Reson Med 2005;53(6):1432–40.
[8] Jensen JH, Helpern JA. MRI quantification of non-Gaussian water diffusion by kurtosis analysis. NMR Biomed 2010;23(7):698–710.
[9] Zhuo J, Xu S, Proctor JL, Mullins RJ, Simon JZ, Fiskum G, et al. Diffusion kurtosis as an in vivo imaging marker for reactive astrogliosis in traumatic brain injury. NeuroImage 2012;59(1):467–77.
[10] Wang ML, Yu MM, Yang DX, Liu YL, Wei XE, Li WB. Diffusion kurtosis imaging characterizes brain microstructural changes associated with cognitive impairment in a rat model of chronic traumatic brain injury. Neuroscience 2018;392:180–9.
[11] Heye AK, Culling RD, Valdes Hernandez Mdel C, Thrippleton MJ, Wardlaw JM. Assessment of blood-brain barrier disruption using dynamic contrast-enhanced MRI. A systematic review. NeuroImage Clin 2014;6:262–74.
[12] Wei XE, Wang D, Li MH, Zhang YZ, Li YH, Li WB. A useful tool for the initial assessment of blood-brain barrier permeability after traumatic brain injury in rabbits: dynamic contrast-enhanced magnetic resonance imaging. J Trauma 2011;71(6):1645–50. [discussion 50-1].
[13] Wei XE, Zhang YZ, Li YH, Li MH, Li WB. Dynamics of rabbit brain edema in focal lesion and perilesion area after traumatic brain injury: a MRI study. J Neurotrauma 2012;29(14):2413–20.
[14] Yoo RE, Choi SH, Oh BM, Do Shin S, Lee EJ, Shin DJ, et al. Quantitative dynamic contrast-enhanced MR imaging shows widespread blood-brain barrier disruption in mild traumatic brain injury patients with post-concussion syndrome. Eur Radiol 2018;29(3):1308–17.
[15] Wang ML, Yu MM, Yang DX, Liu YL, Wei XE, Li WB. Longitudinal microstructural changes in traumatic brain injury in rats: a diffusional kurtosis imaging, histology,

and behavior study. AJNR Am J Neuroradiol 2018;39(9):1650–6.
[16] Li W, Watts L, Long J, Zhou W, Shen Q, Jiang Z, et al. Spatiotemporal changes in blood-brain barrier permeability, cerebral blood flow, T2 and diffusion following mild traumatic brain injury. Brain Res 2016;1646:53–61.
[17] Romine J, Gao X, Chen J. Controlled cortical impact model for traumatic brain injury. J Vis Exp 2014;90:e51781.
[18] Liu YL, Yuan F, Yang DX, Xu ZM, Jing Y, Yang GY, et al. Adjudin attenuates cerebral edema and improves neurological function in mice with experimental traumatic brain injury. J Neurotrauma 2018;35(23):2850–60.
[19] Tabesh A, Jensen JH, Ardekani BA, Helpern JA. Estimation of tensors and tensor-derived measures in diffusional kurtosis imaging. Magn Reson Med 2011;65(3):823–36.
[20] Yushkevich PA, Piven J, Hazlett HC, Smith RG, Ho S, Gee JC, et al. User-guided 3D active contour segmentation of anatomical structures: significantly improved efficiency and reliability. NeuroImage 2006;31(3):1116–28.
[21] Tofts PS, Brix G, Buckley DL, Evelhoch JL, Henderson E, Knopp MV, et al. Estimating kinetic parameters from dynamic contrast-enhanced T(1)-weighted MRI of a diffusable tracer: standardized quantities and symbols. J Magn Reson Imaging 1999;10(3):223–32.
[22] Obermeier B, Daneman R, Ransohoff RM. Development, maintenance and disruption of the blood-brain barrier. Nat Med 2013;19(12):1584–96.
[23] Chen S, Pickard JD, Harris NG. Time course of cellular pathology after controlled cortical impact injury. Exp Neurol 2003;182(1):87–102.
[24] Susarla BT, Villapol S, Yi JH, Geller HM, Symes AJ. Temporal patterns of cortical proliferation of glial cell populations after traumatic brain injury in mice. ASN Neuro 2014;6(3):159–70.
[25] Umesh Rudrapatna S, Wieloch T, Beirup K, Ruscher K, Mol W, Yanev P, et al. Can diffusion kurtosis imaging improve the sensitivity and specificity of detecting microstructural alterations in brain tissue chronically after experimental stroke? Comparisons with diffusion tensor imaging and histology. NeuroImage 2014;97:363–73.
[26] Hazra A, Macolino C, Elliott MB, Chin J. Delayed thalamic astrocytosis and disrupted sleep-wake patterns in a preclinical model of traumatic brain injury. J Neurosci Res 2014;92(11):1434–45.
[27] Huh JW, Widing AG, Raghupathi R. Midline brain injury in the immature rat induces sustained cognitive deficits, bihemispheric axonal injury and neurodegeneration. Exp Neurol 2008;213(1):84–92.
[28] Zhou Y, Lui YW, Zuo XN, Milham MP, Reaume J, Grossman RI, et al. Characterization of thalamo-cortical association using amplitude and connectivity of functional MRI in mild traumatic brain injury. J Magn Reson Imaging 2014;39(6):1558–68.
[29] Ross DT, Ebner FF. Thalamic retrograde degeneration following cortical injury: an excitotoxic process? Neuroscience 1990;35(3):525–50.
[30] Little DM, Kraus MF, Joseph J, Geary EK, Susmaras T, Zhou XJ, et al. Thalamic integrity underlies executive dysfunction in traumatic brain injury. Neurology 2010;74(7):558–64.
[31] Jones EG. Synchrony in the interconnected circuitry of the thalamus and cerebral cortex. Ann N Y Acad Sci 2009;1157:10–23.
[32] Grossman EJ, Ge Y, Jensen JH, Babb JS, Miles L, Reaume J, et al. Thalamus and cognitive impairment in mild traumatic brain injury: a diffusional kurtosis imaging study. J Neurotrauma 2012;29(13):2318–27.
[33] Gong NJ, Kuzminski S, Clark M, Fraser M, Sundman M, Guskiewicz K, et al. Microstructural alterations of cortical and deep gray matter over a season of high school football revealed by diffusion kurtosis imaging. Neurobiol Dis 2018;119:79–87.
[34] Grossman EJ, Jensen JH, Babb JS, Chen Q, Tabesh A, Fieremans E, et al. Cognitive impairment in mild traumatic brain injury: a longitudinal diffusional kurtosis and perfusion imaging study. AJNR Am J Neuroradiol 2013;34(5):951–7. [s1–3].
[35] Mouzon BC, Bachmeier C, Ferro A, Ojo JO, Crynen G, Acker CM, et al. Chronic neuropathological and neurobehavioral changes in a repetitive mild traumatic brain injury model. Ann Neurol 2014;75(2):241–54.
[36] Gong NJ, Wong CS, Chan CC, Leung LM, Chu YC. Correlations between microstructural alterations and severity of cognitive deficiency in Alzheimer's disease and mild cognitive impairment: a diffusional kurtosis imaging study. Magn Reson Imaging 2013;31(5):688–94.